# Effective theory for graphene nanoribbons with junctions

Johann Ostmeyer,[1,*] Lado Razmadze,[2,†] Evan Berkowitz,[2,3,4,‡] Thomas Luu,[2,5,§] and Ulf-G. Meißner[2,4,5,6,‖]

[1]*Department of Mathematical Sciences, University of Liverpool, Liverpool L69 7ZL, United Kingdom*
[2]*Institute for Advanced Simulation (IAS-4), Forschungszentrum Jülich, Germany*
[3]*Jülich Supercomputing Center, Forschungszentrum Jülich, 54245 Jülich, Germany*
[4]*Center for Advanced Simulation and Analytics (CASA), Forschungszentrum Jülich, 52425 Jülich, Germany*
[5]*Helmholtz-Institut für Strahlen- und Kernphysik and Bethe Center for Theoretical Physics, Rheinische Friedrich-Wilhelms-Universität Bonn, Germany*
[6]*Tbilisi State University, 0186 Tbilisi, Georgia*

(Received 9 February 2024; revised 17 April 2024; accepted 22 April 2024; published 10 May 2024)

Graphene nanoribbons are a promising candidate for fault-tolerant quantum electronics. In this scenario, qubits are realized by localized states that can emerge on junctions in hybrid ribbons formed by two armchair nanoribbons of different widths. We derive an effective theory based on a tight-binding ansatz for the description of hybrid nanoribbons and use it to make accurate predictions of the energy gap and nature of the localization in various hybrid nanoribbon geometries. We use quantum Monte Carlo simulations to demonstrate that the effective theory remains applicable in the presence of Hubbard interactions. We discover, in addition to the well-known localizations on junctions, which we call "Fuji", a new type of "Kilimanjaro" localization smeared out over a segment of the hybrid ribbon. We show that Fuji localizations in hybrids of width $N$ and $N+2$ armchair nanoribbons occur around symmetric junctions if and only if $N \pmod 3 = 1$, while edge-aligned junctions never support strong localization. This behavior cannot be explained relying purely on the topological $Z_2$ invariant, which has been believed to be the origin of the localizations to date.

DOI: 10.1103/PhysRevB.109.195135

## I. INTRODUCTION

The ability to engineer hybrid nanoribbons [1,2] has opened up the possibility of using such systems to manufacture quantum dots [3] and other advanced electronic devices. A central aspect that drives the usefulness of these systems is their ability to support localized electronic states that can be achieved through careful doping of the ribbons. Various models of nanoribbons exhibit edge-state localization with a topological origin [4–7]. In Ref. [8] it was argued that completely localized low-energy states occur at the junction of two armchair graphene nanoribbons (AGNRs) that are topologically distinct, forming so-called symmetry-protected topological edge states that should depend only on the geometrical, or topological, aspects of the system and not on the details of any interaction. These states have electrons confined not only to the edge of the ribbon, but concentrated around the junctions.

Reference [9] confirmed that this localization is robust against the inclusion of an on-site Hubbard interaction via nonperturbative calculations. The localization of states for the 7/9 and 13/15 hybrid nanoribbon systems persisted for a wide range of Hubbard interactions. Recently the authors of Ref. [10] have also investigated the role of interactions in ribbons with finite lengths using a mean-field prescription. Other interesting phenomena occur when certain symmetries, such as the sublattice or *chiral* symmetry, is broken in these systems [11].

Although states in these hybrid systems demonstrate localization originating at junctions between different distinct AGNRs, the exact asymptotic behavior of these localized states has not been quantified. As a function of distance from a junction wavefunctions may fall off exponentially ("strong localization") or with some power law ("weak localization"). This distinction has ramifications for the engineering requirements for manufacturing ribbons that support localization. As we show in this paper, ribbon junctions that support wavefunctions with exponential decays on either side can be constructed such that they are nearly gapless under the tight-binding approximation. Further, localization in this case can occur for a hybrid system with a single junction.

On the other hand, weak localization on either side of the ribbon junction cannot support a zero mode. Using weak localization to concentrate a state along a ribbon segment requires ribbons with an even number of junctions.

These findings are easily understood through an effective theory (ET) of the hybrid ribbons in one dimension (1D).

*j.ostmeyer@liverpool.ac.uk
†l.razmadze@fz-juelich.de
‡e.berkowitz@fz-juelich.de
§t.luu@fz-juelich.de
‖meissner@hiskp.uni-bonn.de

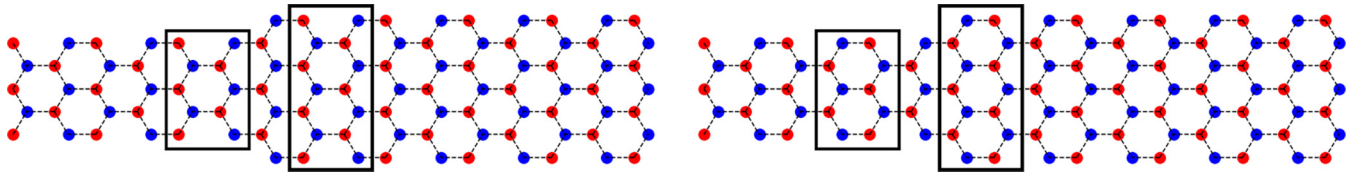

FIG. 1. A symmetric 5/7-junction made from the intersection of a 5-AGNR and a 7-AGNR. The solid rectangles highlight the unit cells of the two individual AGNRs, with two different but equivalent choices shown in the left and right panels. The junction resides between the two unit cells shown, respectively. Note that the central junction has an additional lattice point residing on the blue sublattice compared to the red sublattice in both cases, as described in the text. The central junction and the junction on the edge of the compound unit cell can be thought of as a single unit cell divided in two.

We show how to construct such a theory, and demonstrate how the parameters of this ET can be tuned to reproduce the low-energy spectrum of hybrid ribbons, even in the presence of nonperturbative interaction. Once tuned, it is much simpler to use this theory to ascertain the behavior of the low-energy spectrum of these systems for different ribbon lengths. Indeed, we use this ET to make predictions on the specifications of hybrid ribbons that lead to a (nearly) gapless system. We verify the predictions of our ET by comparing directly with calculations on the original hybrid systems.

Our paper is organized as follows. In Sec. II we review ribbons of uniform width and their noninteracting dispersion relations; whether a given width is gapped or not controls how electronic states are localized around the junctions of hybrid ribbons, which we demonstrate in Sec. III. If a uniform ribbon is gapped the wavefunction decays exponentially on a segment of that width near a junction, while if the uniform ribbon is not gapped the wavefunction decays only with an inverse power law. From this understanding we develop and test an effective one-dimensional tight-binding Hamiltonian with two hopping amplitudes in Sec. IV. We show how the effective hopping amplitudes depend on the specific geometries of the hybrid ribbons, identifying low-energy constants (LECs) that depend on the width of the ribbon segments but not on their lengths. After fitting these LECs we demonstrate how our ET predicts ribbon widths and lengths that have a nearly gapless spectrum. We extend the validity of the ET to hybrid ribbons with Hubbard interaction by introducing an additional LEC and verify correctness using quantum Monte Carlo simulations. After commenting on hybrid ribbons not aligned along their centers, we recapitulate in Sec. V.

## II. RIBBONS OF UNIFORM WIDTH

Armchair graphene nanoribbons (AGNRs) are carbon nanostructures defined by their edge terminations and can be seen as a portion of an infinite honeycomb lattice with interion spacing $a$. The ribbons enjoy a translational symmetry along their length, which generates a lattice momentum $k$. The width $N$ of an AGNR is the number of ions along a zigzag path across the ribbon, and a single unit cell consists of two neighboring transverse zigzags. A ribbon of $m$ unit cells can be compactified with periodic boundary conditions at its ends. Figure 1 shows two ribbon segments of widths 5 and 7 joined at a junction. Clearly both segments as well as the complete hybrid ribbon have a bipartite structure where ions of one triangular sublattice (colored blue) have neighbors only on the other sublattice (colored red) and vice versa.

In order to understand how the geometry influences the strength of electronic state localizations, we have to investigate the energy spectra of the different armchair ribbons themselves. Of interest will be the state that is closest to zero energy, since this state will govern the long-range correlations. A gapped system has a finite correlation length while an ungapped system has infinite correlations, cut off in practice by the physical length of the ribbon.

With nearest-neighbor-hopping amplitude $\kappa$ these systems are described by the Hamiltonian

$$H = -\kappa \sum_{\langle x,y \rangle} (\psi_x^\dagger \psi_y + \psi_y^\dagger \psi_x) + \text{interactions}, \tag{1}$$

where $\psi_x$ destroys an electron at site $x$, with $x$ and $y$ are on different sublattices, and we suppress spin labels here and henceforth. When the interactions are neglected, $H$ is just the tight-binding Hamiltonian used to describe the band structure [12,13] and we can find energy eigenstates by diagonalizing the adjacency matrix.

The dispersion relations of armchair ribbons of widths 5 to 8 described by this Hamiltonian are shown in Fig. 2. The armchair ribbons with widths $N = 5$ and $N = 8$ are gapless while the widths $N = 6$ and $N = 7$ have finite gaps. This reflects the well-known fact that armchair ribbons are gapless if and only if their width is

$$N \equiv 2 \pmod 3. \tag{2}$$

A general analytic description of the spectrum of these ribbons in the tight-binding model can be found in Ref. [4]. The noninteracting many-body state has all the negative energy states filled.

The authors of [8] enumerated four distinct types of AGNR edge terminations based on ribbon width and inversion and mirror symmetries. They showed that the nanoribbons have an associated binary conserved quantity, the so-called $Z_2$ topological invariant.

## III. HYBRIDS RIBBONS AND JUNCTIONS

Finite ribbon segments of different width can be joined together to form a *hybrid ribbon*. The interface of two materials can support surface modes [14], in this case modes localized along the hybrid ribbon's length. We mention two out of the multitude of possible shapes that hybrid ribbons can have: two semi-infinite segments with only a single junction and repeated segments of alternating widths, with a junction at every width change. If the alternation is regular the two alternating segments form one compound unit cell, which

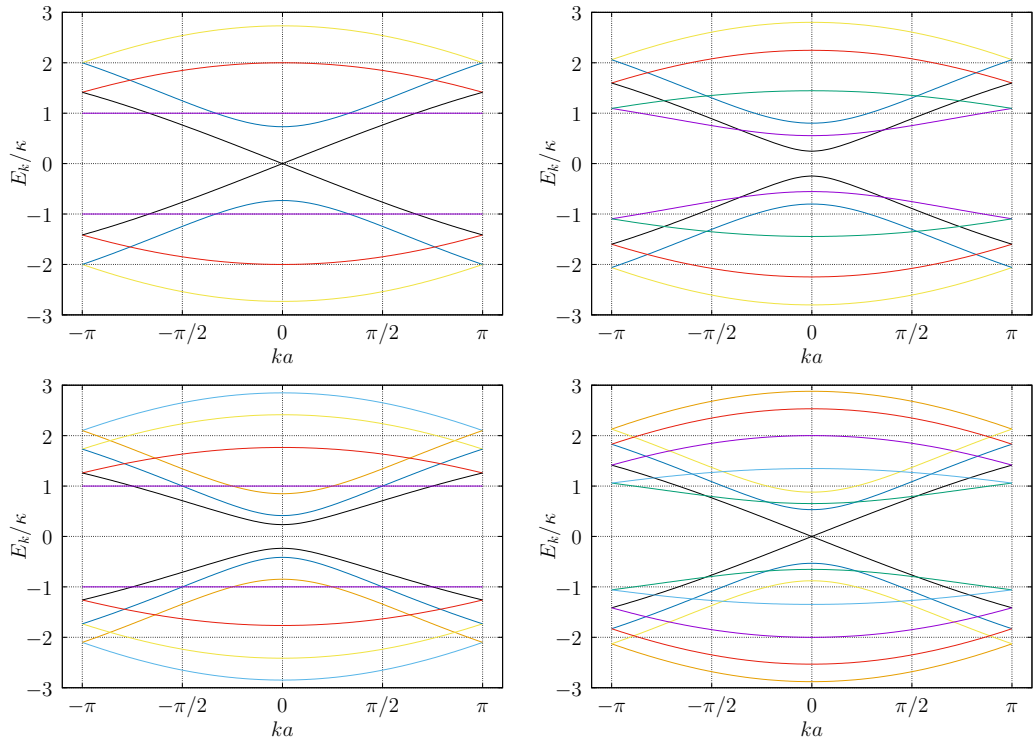


FIG. 2. Dispersion relations of infinitely long (i.e., $m_N = \infty$) armchair ribbons with widths $N = 5, 6, 7, 8$ (top left to bottom right).

may be repeated $L$ times along the hybrid ribbon's length; we reuse $m$ to count the number of unit cells in a segment. The compound unit cell will later be represented by two sites in our effective theory, one site for each junction.

In Ref. [8] it was argued that the topology of these systems preserved the localization of states even under the presence of interactions. Their perturbative calculations corroborated this claim. Consequently in Ref. [9] it was shown numerically that this localization persisted in the nonperturbative regime. In particular, [9] investigated the 7/9 hybrid (and the 13/15 hybrid) nanoribbon with nonperturbative stochastic methods and found that localization indeed persisted in the presence of a Hubbard interaction. One goal of this present paper is to better quantify the nature of these localized states for not only the 7/9 geometry, but for other hybrid nanoribbon geometries. As we show in later sections, the dynamics of these low-energy states can be captured in a simple effective 1D model, which in turn allows us to make predictions for a broader range of hybrid nanoribbons.

For simplicity we only consider ribbons segments consisting of a width-$N$ armchair of length $m_N$ and a width-$N+2$ armchair of length $m_{N+2}$ with odd $N$. When ribbon segments of different widths are aligned along their centers, as in Fig. 1, so that the ribbon has a reflection symmetry, the junction has a surplus of a single lattice site, belonging to one of the sublattices (blue in the center of Fig. 1, red at the edge). In this picture it is crucial to tile the hybrid ribbon with unit cells of similar shape in both lattice segments. The two leftover zigzags on the junctions can be understood as a single unit cell divided. While in the left panel of Fig. 1 we choose unit cells that are open at top and bottom, we can equivalently choose all unit cells to be closed as in the right panel. In the former case the surplus lattice site comes from the junction zigzag of the broad segment while in the latter case the surplus resides within the narrow segment, but it always belongs to the same sublattice. This sublattice surplus locally breaks chiral symmetry. We will find later that hybrid ribbons aligned at an edge do not break chiral symmetry.

Figure 3 shows two compound unit cells of an example 7/9 hybrid nanoribbon, where we see the honeycomb lattice, which forms the basis for extended carbon nanostructures. A ribbon of width $N = 7$ has topological invariant $Z_2 = 0$, while a ribbon of width $N + 2 = 9$ has invariant $Z_2 = 1$ (more

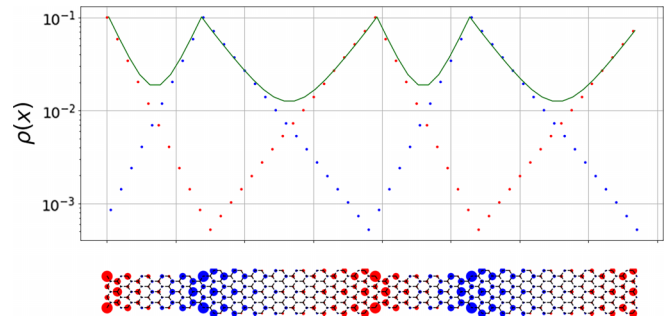


FIG. 3. (Bottom) The Fuji-localized state of a 7/9 hybrid ribbon with $(m_7, m_9) = (5, 8)$, shown with $L = 2$ two unit cells. The circles' radii are proportional to the densities $\rho$ (5) and their color indicates the sublattice. (Top) We sum $\rho$ along the width of the ribbon and color each point colored according to sublattice. The green line is the sum of both red and blue points along one zigzag cross section and represents the total occupancy probability (integrated across the ribbon's width) along the ribbon's length.

TABLE I. Topological invariant [8] (Table I therein) for the narrower and broader parts of different junctions respectively. In a hybrid ribbon with a symmetric junction (Figs. 1 and 3–5), the $Z_2'$ invariant describes the topology in the narrow and $Z_2$ the broader segment. In bottom aligned junctions (Fig. 12) both parts are described by the $Z_2'$ invariant. Reference [8] predicts localizations for junctions with changing topology.

| $N$ | 3 | 5 | 7 | 9 | 11 | 13 | 15 | 17 | 19 | 21 |
|---|---|---|---|---|---|---|---|---|---|---|
| $N+2$ | 5 | 7 | 9 | 11 | 13 | 15 | 17 | 19 | 21 | 23 |
| $Z_2'(N)$ | 1 | 0 | 0 | 0 | 1 | 1 | 1 | 0 | 0 | 0 |
| $Z_2(N+2)$ | 1 | 1 | 1 | 0 | 0 | 0 | 1 | 1 | 1 | 0 |

details in Table I); localization is conjectured to occur at the junctions [8]. This system has been experimentally fabricated [1,2].

Because the geometry controls the gap, a localized state will decay differently on the two sides of the junction. A localized electron's wavefunction $\phi$ should decay with the dimensionless distance from the junction $\Delta x$. With large enough length segment length $m$, we expect the asymptotic decay to be governed by the gap or gaplessness of the infinite ribbon of the same width [15]. In a gapped segment we expect strong localization and exponential decay

$$\phi \sim e^{-\beta \Delta x}, \tag{3}$$

and in a gapless segment we expect monomial decay

$$\phi \sim \Delta x^{-\beta}, \tag{4}$$

and only weak localization. In both cases $\beta$ is some positive width-dependent parameter independent of segment length $m$ and the number of compound unit cells $L$. This dependence on width $N$ has to be determined from fits to solutions of the full problem.

In the bottom panel Fig. 3 we show the lowest positive-energy single-electron tight-binding eigenfunction on a 7/9 hybrid ribbon where the width-7 segments have five unit cells and the width-9 segments have eight unit cells each, $(m_7, m_9) = (5, 8)$. We take the eigenfunction $\phi$ and compute the density normalized per unit cell

$$\rho(x) = |\phi(x)|^2, \quad \frac{1}{L}\sum_x \rho(x) = 1. \tag{5}$$

The radii of the circles are proportional to $\rho$ and colored according to their sublattice. In the top panel we show the marginal densities $\rho(x)$ summed over the width of the ribbon, again coloring according to sublattice. The green line is obtained by adding both the red and blue marginal densities along a transverse zigzag and represents the total occupancy probability along the ribbon's length. Both 7- and 9-armchair ribbons are gapped since neither satisfy the gaplessness condition (2), so correlations decay exponentially on both sides of each junction in Fig. 3.

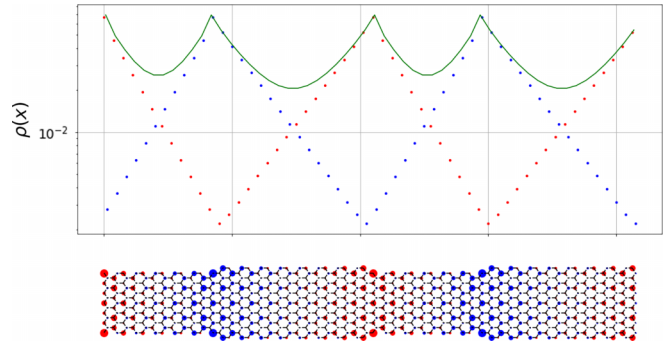


FIG. 4. Similar to Fig. 3 but now the 13/15 hybrid with $(m_{13}, m_{15}) = (6, 8)$.

That the $N = 7$ gap is larger than the $N = 9$ gap is apparent by the faster decay on the width-7 segments. We observe that on neighboring junctions the states are not only localized in space but are also concentrated on one sublattice or the other. The strong exponential localization allows these states to be clearly delineated.

We remark that this junction also has changing topology according to Ref. [8] (see Table I) and their prediction of localization therefore coincides with ours. The same occurs for the 13/15 hybrid system, which we show in Fig. 4. However, we will see that there are counterexamples to the otherwise well-motivated conjecture put forth in Ref. [8] that the localizations are driven purely by the topological $Z_2$ boundary. The model we will develop in Sec. IV is generally applicable and reliably quantifies localizations even in the cases that evade the topological argument.

Figure 5 shows the low-energy states from 3/5, 5/7, and 9/11 hybrid ribbons. Each of these examples has a gapless segment, since $5 \equiv 11 \equiv 2 \pmod 3$ satisfying the gaplessness condition (2), and on the gapless segment no sharp

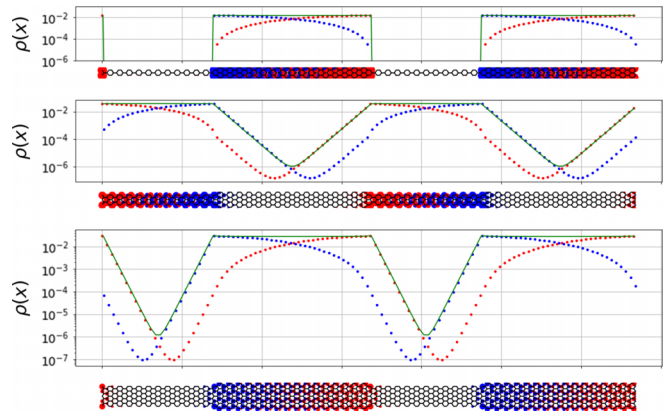


FIG. 5. Lowest energy state densities of a 3/5 (top), a 5/7 (middle), and a 9/11 hybrid (bottom), all with segment lengths $(m_N, m_{N+2}) = (12, 16)$. These examples do not feature the two-sided exponential Fuji localization on the junctions since width-5 and width-11 armchair ribbons have long range correlations. However, the states are trapped within those gapless segments, showing Kilimanjaro localization.

localization on the junction occurs. Instead, on the scale shown the eigenstate looks essentially constant on the gapless segments.

We distinguish these "Kilimanjaro-localized" states with a large plateau from the sharply peaked "Fuji-localized" states that have exponential decay on both sides of a junction [16]. We remark that the cumulated occupancy density shown in green is not exactly constant in the plateau region. Instead, the density increases towards the center. In fact, if the gapless segment is very short, the localization can be very sharp, not unlike Fuji localization. But, the state can also be meaningfully spread over vast regions if the gapless segment is long enough.

Focusing on the 5/7 hybrid, as we make $m_7$ larger the low-energy state remains confined to the width-5 segments. If we take $m_7 \gg m_5$, we can effectively localize the density into an arbitrarily small space compared to the total length of the ribbon. Unlike the Fuji localization, in this limit there is no sharp splitting between the two sublattices. The localization in the gapless segment are only polynomial in nature and states localized to the two sublattices at either end of the gapless segment have a large overlap.

The 5/7 example, in particular, contradicts the claim in Ref. [8] that a change in topology implies a Fuji localization. However, we find that the reverse implication—localization requires a change in topology—is consistent with the examples we have examined and the effective theory we present in Sec. IV.

The findings of Ref. [8] are based on hybrid ribbons with a single junction connected by semi-infinite ends, whereas our investigations here involve hybrid ribbons with periodic boundary conditions, which essentially models an infinite number of junctions. A natural question is whether this difference accounts for the discrepancy between our findings. With our numerical techniques it is not possible to model infinite ribbons. However, instead of periodic boundary conditions at the ends, we can use open boundary conditions and investigate the nature of the localization as we extend the length of each semiribbon. We show the length-normalized densities for the lowest nonzero energy state [17] for increasingly long 5/7 hybrid ribbons with open boundaries in Fig. 6. The Kilimanjaro localization is prominent and remains so as the ribbons' respective lengths increase. We therefore surmise that this type of localization persists in the limit of semi-infinite ends. This is perfectly in line with the expectations in our ET framework and cannot be reconciled with the predictions in Ref. [8].

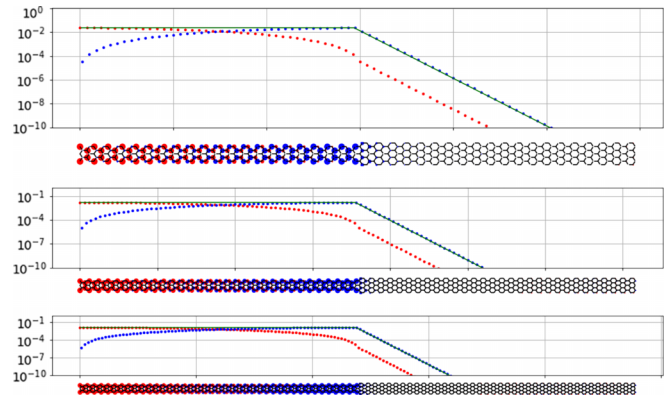

FIG. 6. Lowest nonzero energy state densities of the 5/7 ribbon with open boundary conditions. The top panel has $(m_N, m_{N+2}) = (20, 20)$, middle $(m_N, m_{N+2}) = (30, 30)$, and bottom $(m_N, m_{N+2}) = (40, 40)$. The states are again trapped within those gapless segments and demonstrate Kilimanjaro localization.

## IV. EFFECTIVE 1D TIGHT-BINDING MODEL

### A. Formulation

An electron localized on a junction is smeared out over many sites of one sublattice near by. We observe in Figs. 3–5 that at a junction the wavefunction is concentrated on the sublattice with a surplus site. This sublattice symmetry breaking and wavefunction concentration allows us to treat the $2L$ junctions from $L$ compound unit cells as the sites of our model. Because the junctions alternate between having a surplus of one of the honeycomb sublattices (and the corresponding wavefunction concentration), we arrive at a length $L$ bipartite lattice with a two-site basis. The two effective sites can be thought of as the local surplus of one or the other sublattice. Electrons hop between these effective sites via some hopping amplitude controlled by the width and length of the segment connecting them; a segment of width $N$ and length $m_N$ lets electrons tunnel with an amplitude controlled by the wavefunction overlap. If two junctions are separated by a strongly localizing segment (3) of length $m$ the wavefunction overlap and thus the tunneling amplitude $t$ will be exponentially small,

$$t \sim e^{-\beta m}, \tag{6}$$

while two junctions separated by a weakly localizing segment (4) will have polynomial overlap and tunneling amplitude

$$t \sim m^{-\beta}, \tag{7}$$

redefining the dimensionless $\beta$.

An effective 1D tight-binding Hamiltonian that describes a hybrid ribbon of alternating widths $N$ and $N+2$ is

$$H_{\mathrm{1D}} = -\sum_{x=0}^{L-1} (t_N c_{2x}^\dagger c_{2x+1} + t_{N+2} c_{2x+1}^\dagger c_{2x+2} + \mathrm{H.c.}), \tag{8}$$

where $c_x$ destroys a fermion at effective site $x$, and $t_N$ is the tunneling (or hopping) amplitude across a ribbon segment of width $N$. It can be block-diagonalized by a Fourier transformation yielding

$$H_{\mathrm{1D}} = -\sum_k c_k^\dagger \begin{pmatrix} 0 & t_N e^{\mathrm{i}k} + t_{N+2} e^{-\mathrm{i}k} \\ t_N e^{-\mathrm{i}k} + t_{N+2} e^{\mathrm{i}k} & 0 \end{pmatrix} c_k, \tag{9}$$

where the dimensionless momentum $k$ is in terms of the inverse lattice spacing and the creation and annihilation operators in momentum space are two-dimensional vectors,

$$c_k = \begin{pmatrix} c_{k,A} \\ c_{k,B} \end{pmatrix} \tag{10}$$

and the $A$ and $B$ indices indicate the two sublattices or equivalently the two junctions.

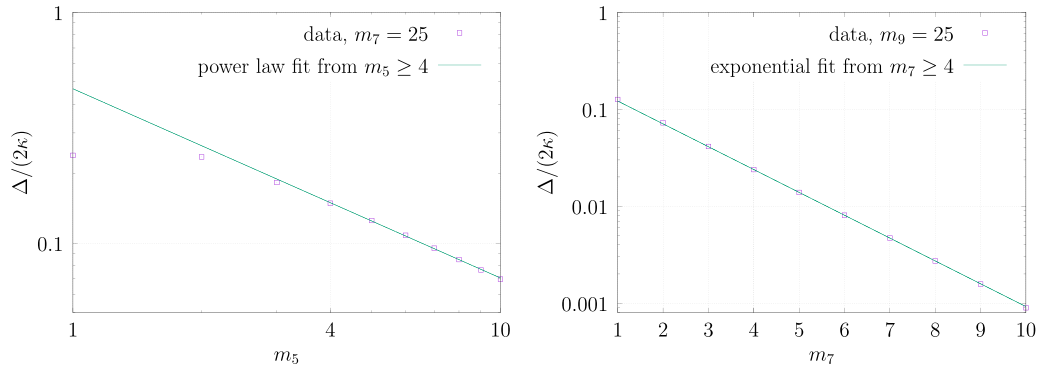


FIG. 7. Gaps of a 5/7 hybrid (left) and a 7/9 hybrid (right) used to fit the LECs (13) for $N = 5$ and $N = 7$, respectively. When fitting a power law as a function of the length $m_5$, the length $m_7 = 25$ has been kept fixed and similarly for the exponential fit to $m_7$ we fixed $m_9 = 25$.

After diagonalizing the blocks we obtain the dispersion relation

$$E(k) = \pm\sqrt{t_N^2 + t_{N+2}^2 + 2t_N t_{N+2}\cos 2k} \tag{11}$$

for momenta in the reduced first Brillouin zone $k \in [0, \pi)$ and the energy gap

$$\Delta \equiv 2|E(\pi/2)| = 2\sqrt{t_N^2 + t_{N+2}^2 - 2t_N t_{N+2}} = 2|t_N - t_{N+2}| \tag{12}$$

between lowest positive and highest negative energies, which will become very important in the following considerations. Note that a hybrid ribbon with small $t_N$ and $t_{N+2}$ necessarily has a small gap. However, a small $t_N$ is a consequence of a large pure-armchair gap since in this case it less likely to hop between junctions. This effective theory predicts that joining two strongly gapped ribbons leads to a very small overall gap.

Sharpening the scaling of the overlaps (6) and (7) into quantitative predictions, the effective hopping amplitudes are

$$t_N(m) = \begin{cases} \kappa\,\alpha\, m^{-\beta} & \text{with } \beta \sim 1, \quad \text{if} \quad N = 2 \pmod 3, \\ \kappa\,\alpha\, e^{-\beta m} & \text{with } \beta \sim \Delta_N, \quad \text{otherwise}, \end{cases} \tag{13}$$

with $\alpha$ another (*apriori* unknown) positive dimensionless parameter that can only depend on $N$, not on $m$ and $L$ and the honeycomb $\kappa$ (1) appears for dimensional reasons. In the first case $\beta$ is expected to be related to critical behavior and cannot be predicted from first principles. In contrast, the exponential decay is governed by the magnitude of the pure $N$-armchair ribbon gap $\Delta_N$ up to small corrections. We will use this ansatz to fit the low-energy constants (LECs) $\alpha$ and $\beta$ for different values of $N$.

Concisely, the effective treatment predicts that an $N/N+2$ hybrid ribbon of two armchair nanoribbons has Fuji-localized states with close to zero energy if and only if the junction is center aligned and $N \pmod 3 = 1$ so that neither width fulfils the gaplessness condition (2).

### B. Determination of the low-energy constants

We now have all ingredients to fix the low-energy constants (13) of our 1D effective theory (8). By considering a particular $N/N+2$ hybrid ribbon, we calculate the gap $\Delta$ (defined as twice the lowest positive single-particle energy) of the hybrid system for different ribbon lengths $m_N$ and $m_{N+2}$. For the sake of simplicity we choose one of the lengths very large, say $m_{N+2} \gg m_N$, so that the $N+2$-width ribbon segment is long enough to be compatible with the thermodynamic limit. Then the effects of this ribbon segment are negligible and the junction gap (12) reduces to $\Delta = 2t_N$. We fit our results for $t_N(m_N)$ to the form of the effective hopping (13), fixing the parameters $\alpha_N$ and $\beta_N$. Two representative fits are shown in Fig. 7, with a power-law fit in the left panel and an exponential fit on the right.

We summarize the results of the fitted low-energy constants in Table II for select values of $N$. Within either class, power law or exponential, we observe the trend that both LECs $\alpha$ and $\beta$ decrease with growing $N$. While we do not have a direct physical interpretation for the proportionality constant $\alpha$, it is clear that $\beta$ has to follow this trend because the asymptotic $N \to \infty$ case of graphene is gapless. In particular, the exponential case features decay coefficients $\beta$ similar to the pure armchair ribbon gap $\Delta_N$ as expected.

Note how the 7/9-junction is special in the sense that it is the smallest ribbon size with strong localization for both widths. No Fuji localization is possible in narrower center-aligned ribbons. We also remark that the 3-armchair ribbon features such a strong exponential decay that it is virtually instant and (at least within double floating precision) $t_3(m) = 0$ for $m > 0$. Localized states do not penetrate into the 3-armchair at all.

TABLE II. Fitted low-energy constants (LECs) $\alpha$, $\beta$ from Eq. (13) following the exponential (exp) or power (pow) laws depending on the width $N$ of the armchair ribbon. $\Delta_N$ is the corresponding energy gap of the ribbon without junction. For $N = 3$ we have $\beta = \infty$ and there is no value for $\alpha$ since the wavefunction is exactly confined to the junction (see Fig. 5).

| $N$ | 3 | 5 | 7 | 9 | 11 | 13 | 15 | 17 | 19 | 21 |
|---|---|---|---|---|---|---|---|---|---|---|
| Decay | exp | pow | exp | exp | pow | exp | exp | pow | exp | exp |
| $\alpha$ | | 0.57 | 0.21 | 0.22 | 0.43 | 0.13 | 0.15 | 0.32 | 0.09 | 0.11 |
| $\beta$ | $\infty$ | 0.89 | 0.54 | 0.34 | 0.79 | 0.30 | 0.23 | 0.69 | 0.22 | 0.18 |
| $\Delta_N$ | 0.83 | 0 | 0.47 | 0.35 | 0 | 0.26 | 0.22 | 0 | 0.18 | 0.16 |

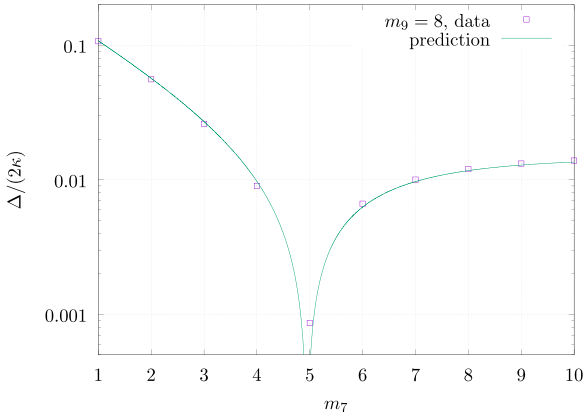


FIG. 8. Gap of a 7/9 hybrid ribbon given by the prediction (14) and direct diagonalization of the underlying tight-binding Hamiltonian shown in (1) (without interactions).

### C. Application of our effective theory

Despite the simplicity of our effective theory, we can already use it to make predictions in cases where the original system is more difficult to simulate. We can apply our ET, for example, to predict the respective lengths at which the gap of a hybrid nanoribbon (almost) vanishes. As an example we return to our prototypical 7/9 hybrid system, but with the desire to pick segment lengths so that the system is as close as possible to gapless.

To minimize the gap (12) our ET provides the condition

$$t_7 \stackrel{!}{=} t_9 \Rightarrow \alpha_7 e^{-\beta_7 m_7} \stackrel{!}{=} \alpha_9 e^{-\beta_9 m_9}$$
$$\Rightarrow m_7 = \frac{\beta_9}{\beta_7} m_9 + \ln \frac{\alpha_7}{\alpha_9} \tag{14}$$

has to hold as best possible for integers $m_7$ and $m_9$. Using the parameters given in Table II we find that $(m_7, m_9) = (5, 8)$ is a good tuple that nearly satisfies this constraint. This prediction is confirmed in Fig. 8, which shows the hybrid ribbon's gap as a function of the width-7 segments' length, holding the width-9 segments at $m_9 = 8$. The next three smallest tuples that our theory predicts for this system are (22,35), (39,62), and (56,89). For the 13/15 hybrid system our effective theory predicts the following four smallest tuples giving a near zero gap: $(m_{13}, m_{15}) = (6, 8)$, (29,38), (52,68), and (75,98).

Note that in both these systems, both ribbon widths are gapped and the localization is Fuji. For systems where one width is gapped and the the other is not, our theory predicts that such systems cannot support a (near) zero gap without weakly localizing segments many orders of magnitude longer than the strongly localizing segments. This is consistent with all our simulations to date.

### D. Incorporating interactions

So far we have focused on noninteracting tight-binding dynamics, both within the hybrid nanoribbon and its effective 1D description. Including interactions, for example by adding an on-site Hubbard interaction $U$ that couples the spin-up $\uparrow$ and spin-down $\downarrow$ electrons

$$H_{\text{Hubbard}} = U \sum_x \left(\psi^\dagger_{x,\uparrow}\psi_{x,\uparrow} - \frac{1}{2}\right)\left(\psi^\dagger_{x,\downarrow}\psi_{x,\downarrow} - \frac{1}{2}\right) \tag{15}$$

to the underlying tight-binding Hamiltonian (1), precludes simple diagonalization.

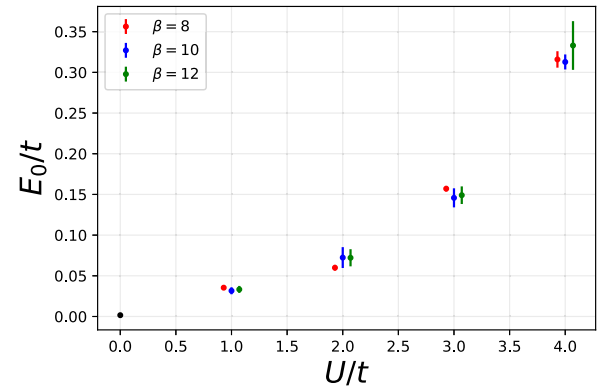


FIG. 9. Interacting energy $E_0$, depicted as points with error bars, of the lowest state as a function of on-site Hubbard interaction $U$ obtained from QMC calculations in Ref. [9] for the 7/9 system with $(m_7, m_9) = (3, 5)$. The 7/9 simulations were performed with three different values of inverse temperature $\beta$, where $\beta = 8$ (12) results are slightly shifted to the left (right) to help visually differentiate the points. The black point corresponds to the noninteracting result.

Reference [9] showed that the localization was robust against the influence of the Hubbard interaction (15) via stochastic Monte Carlo methods and that there is a nearly quadratic dependence of the gap on $U$. Figure 9 shows this dependence for the example of the 7/9 system.

Our 1D effective model (8) can easily incorporate these results by including

$$m_s(c^\dagger_{2x}c_{2x} - c^\dagger_{2x+1}c_{2x+1}), \tag{16}$$

where the effective staggered mass $m_s$ is an LEC and fit to reproduce the quadratic dependence. The momentum-space formulation (9) becomes

$$H_{\text{1D}} = -\sum_k c^\dagger_k \begin{pmatrix} m_s & t_N e^{ik} + t_{N+2}e^{-ik} \\ t_N e^{-ik} + t_{N+2}e^{ik} & -m_s \end{pmatrix} c_k, \tag{17}$$

which can be easily diagonalized, giving

$$E(k) = \pm\sqrt{t_N^2 + t_{N+2}^2 + 2t_N t_{N+2}\cos 2k + m_s^2}, \tag{18}$$

and a gap

$$\Delta = 2|E(\pi/2)| = 2\sqrt{(t_N - t_{N+2})^2 + m_s^2}. \tag{19}$$

The presence of this staggered mass does not change the scaling behavior of the hopping terms (13) and therefore does not affect the nature of the localization. For a given $U$ simulated with a particular tuple $(m_N, m_{N+2})$, the parameter $m_s$ can be tuned so that our ET matches the energy of the underlying theory, like that shown in Fig. 9. Once tuned, we can then make predictions for the size of the gap for hybrid ribbons with segments of the same widths but with different lengths.

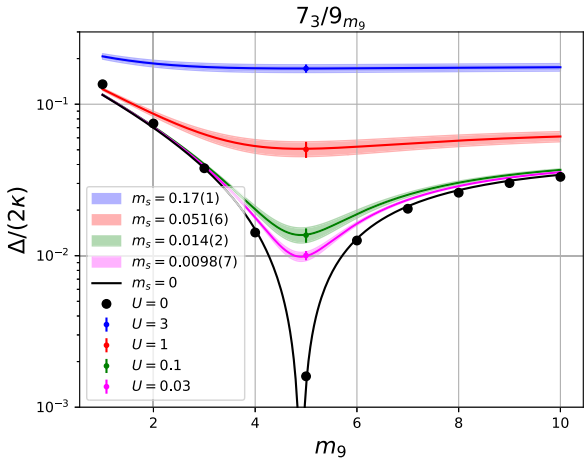


FIG. 10. Extracting $m_s$ from the underlying theory. Here stochastic simulations of the full 7/9 hybrid system with tuple $(m_7, m_9) = (3, 5)$, $L = 1$ and inverse temperature $\beta = 8$ were performed at different values of $U$ as labeled in the figure and shown as points with error bars. The value of $m_s$ was fitted to each of these points, and the resulting prediction of the gap provided by our ET [Eq. (19)] for other tuples where $m_7 = 3$ and $m_9 \in [1, 10]$ is plotted. The black points are the noninteracting results.

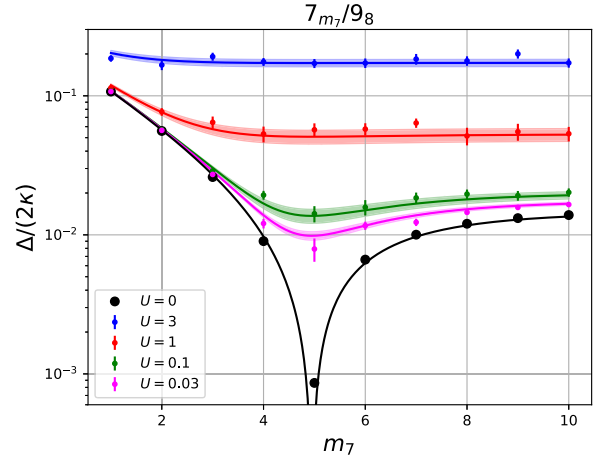


FIG. 11. Comparing our ET prediction with the underlying theory. Using the values of $m_s$ extracted in Fig. 10, we plot our ET prediction of the gap, shown as bands, for 7/9 geometries where $m_9 = 8$ and $m_7 \in [1, 10]$. Superimposed on these bands are the gaps obtained from stochastic simulations of the underlying theory of these systems.

The tuple that minimizes the gap will be the one that corresponds to $|t_N - t_{N+2}| \sim 0$. Since the staggered mass preserves the scaling behavior of the hopping terms, the predicted tuples that minimize the gap in the previous section when $m_s = 0$ will also minimize the gap for $m_s \neq 0$. However, in this case the minimum gap becomes $\Delta \sim 2m_s$.

As an example of how we can extract $m_s$, we perform stochastic simulations of the underlying Hubbard theory on the full 7/9 hybrid ribbon with tuplet $(m_7, m_9) = (3, 5)$. The details of our quantum Monte Carlo (QMC) simulations are described in [9]. In short, we sample the electron configurations from their quantum mechanical probability distribution using a Markov chain with global updates. In the limit of high statistics these simulations become exact. Given limited computational resources, we arrive at a distribution of values around the true result and we depict the standard error of this distribution as error bars in Figs. 9–11.

The results of the gap for different values of Hubbard coupling $U$ are shown as points with error bars in Fig. 10. We then fit our ET to these results, thereby extracting $m_s$ with the values shown in Fig. 10. With $m_s$ in hand, we can predict the value of the gap for other combinations of segment lengths, shown by bands in the same figure.

To demonstrate the efficacy of our ET, we use these same values of $m_s$ to plot our predicted gaps for completely different 7/9 geometries, with $m_9 = 8$, in Fig. 11. Every band in Fig. 11 is a prediction given the low-energy constants $\alpha$ and $\beta$ from the noninteracting case and the effective staggered mass $m_s$ for that Hubbard coupling. In particular, the $(m_7, m_9) = (3, 5)$ hybrid geometry used to extract $m_s$ does not appear in Fig. 11 at all. We then perform stochastic simulations of the underlying theory of these systems and plot their resulting gaps, shown as data points with error bars. We find good agreement between our simulations and ET. We thus surmise that our ET with a staggered mass captures both the dynamics and interactions of the lowest energy spectrum of the hybrid nanoribbons.

More quantitative descriptions of interacting hybrid nanoribbons, potentially going beyond Hubbard interactions, are possible within our formalism. For example, the inclusion of off-diagonal superconducting pairing terms, i.e., $c_k c_k$ and $c_k^\dagger c_k^\dagger$, may be done with the aid of a Bogoliubov transformation [18]. One could alter the dynamics of the system by including next-to-nearest-neighbor hoppings, or extend the interaction by considering on-site plus nearest-neighbor couplings (i.e., extended Hubbard). Such possibilities are the subject of future investigations.

### E. Misaligned hybrid ribbons

In the hybrid ribbons discussed so far the segments are aligned along their center. In Fig. 12 we show junctions aligned along the bottom edge. Unlike the center-aligned hybrids, the junctions of these edge-aligned hybrids do not have surplus of one sublattice or the other and do not break the local sublattice symmetry. This can be seen by tiling the entire hybrid ribbon with similar unit cells (closed at top and bottom as in the right panel of Fig. 1) so that no junction zigzag remains. Strictly speaking, our ET breaks down in this case because no effective lattice site is generated.

Because the sublattice symmetry is locally maintained, there is no local surplus of either sublattice and we predict that no Fuji localization is possible. This is indeed what we observe in both cases of 7/9 and 9/11 edge-aligned junctions. The latter has a change in topology as can be seen in Table I and thus poses another counterexample to the conjecture in Ref. [8]. We identify these states as another realization of Kilimanjaro-localization; the state concentrates into the segment with the smaller gap.

For hybrids whose segments' widths differ by more than 2 some offsets will maintain the sublattice symmetry and some

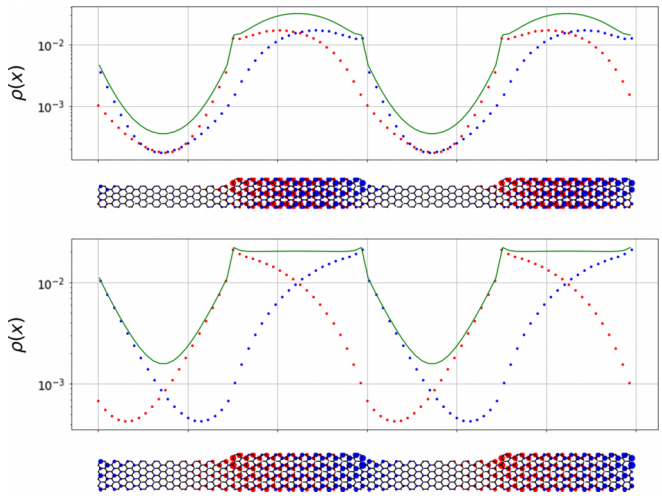


FIG. 12. Lowest energy state densities of a 7/9-junction (top) and a 9/11-junction (bottom) with $(m_N, m_{N+2}) = (10, 10)$ and aligned at the bottom rather than the center. According to Ref. [8] the 9/11-junction features a change in the topology of the respective armchairs (see Table I). Both cases are Kilimanjaro-localized since the 9- and 11-armchair sides, respectively, exhibit long range correlations.

will not. We leave a detailed study of these scenarios to future work.

## V. CONCLUSIONS

When two armchair graphene nanoribbons (AGNRs) of different widths are joined symmetrically (see e.g., Fig. 3), the combined system can feature a smaller band gap than either of the AGNRs and the state with energy closest to zero is localized at the junction. Such a localization can either be strong with correlations decaying exponentially, or weak with a mere power-law decay of correlations (typically not considered localized). We showed that the nature of this localization depends solely on the band gaps of the AGNRs at either side of the junction. More specifically, the localization is strong on one side of the junction if and only if the AGNR on this side has a nonzero gap. This in turn is the case if and only if the ribbon is of width $N \neq 2 \pmod 3$.

We discovered that, in addition to localizations on junctions, a different type of localization is also possible, namely a state localized within a hybrid ribbon segment as shown in Fig. 5. We dub the former type of localizations "Fuji" and the latter "Kilimanjaro". Fuji localizations require exponential correlation decay on both sides of the junction, therefore they are only realized by symmetric $N/N+2$ junctions with $N \pmod 3 = 1$. Kilimanjaro localizations are much more common in that they appear in all $N/N+2$ hybrid AGNRs (symmetric and nonsymmetric, see Fig. 12) without Fuji localization. We observed that these results often coincide with the topology based conjecture for Fuji localizations put forward in Ref. [8]; however, we have also identified counterexamples to the predictions from topology arguments while our description is more fundamental and rigorous for all $N/N+2$ hybrid AGNRs with odd $N$.

We have derived a very simple way to predict and accurately quantify the different types of localized bound states appearing in hybrid AGNRs. For this we reduce the initial two-dimensional tight-binding problem to a one-dimensional effective theory (ET) where the junctions of the hybrid AGNR form the sites of the 1D lattice. The ET also relies on a tight-binding Hamiltonian (8), which is diagonalized analytically and the hopping amplitude between two junctions is defined solely by the ribbon connecting these junctions. Equation (13) summarises this dependence. The hopping decays exponentially with ribbon length for gapped ribbons, signifying strong localization, and it decays as a power law for gapless ribbons resulting in weak localization. We have identified two parameters $\alpha, \beta$, so-called low-energy constants (LECs), in this description that depend only on the width of the AGNR and cannot be determined other than through fitting. We have performed these fits for odd ribbon widths up to $N \leqslant 21$ and summarized the results in Table II. The same fitting procedure can easily be extended to arbitrarily broad ribbons, limited only by computing resources. Once the LECs are determined, they can be used to predict the band gap in hybrid AGNRs, for instance yielding tuples of respective ribbon segment lengths with the smallest gap.

Finally, we put forth an extension of our ET in the presence of Hubbard type interactions (15). Consistent with previous findings [9], we predict the localizations to persist in the presence of interaction and we furthermore describe the quadratic dependence of the gap on the Hubbard interaction using an effective staggered mass term as a third LEC.

Localized Fuji-type states in armchair nanoribbons have been proposed as qubit candidates for fault-tolerant quantum computing before [1,3,8,9] (nicely explained and visualized in Ref. [19]). Their stability against perturbations make them very promising for this application. We now add that Kilimanjaro-localized states are also well suited for the same task and they even might have some advantages, for instance that Fuji localizations come in alternating shapes while all Kilimanjaro localizations are symmetric and thus equivalent. Moreover, while localized Fuji states for a particular junction type always have the same extent, Kilimanjaro states can be smeared out over virtually arbitrary lengths, purely governed by the length of the confining ribbon segment.

## ACKNOWLEDGMENTS

This work was supported in part by the Chinese Academy of Sciences (CAS) President's International Fellowship Initiative (PIFI) (Grant No. 2018DM0034) and Volkswagen Stiftung (Grant No. 93562). It was also funded in part by the STFC Consolidated Grant No. ST/T000988/1 and the Deutsche Forschungsgemeinschaft (DFG, German Research Foundation) as part of the CRC 1639 NuMeriQS Project No. 511713970. Finally, we gratefully acknowledge the computing time granted by the JARA Vergabegremium and provided on the JARA Partition part of the supercomputer JURECA at Forschungszentrum Jülich.

[1] D. J. Rizzo, G. Veber, T. Cao, C. Bronner, T. Chen, F. Zhao, H. Rodriguez, S. G. Louie, M. F. Crommie, and F. R. Fischer, Topological band engineering of graphene nanoribbons, Nature (London) **560**, 204 (2018).

[2] O. Gröning, S. Wang, X. Yao, C. A. Pignedoli, G. Borin Barin, C. Daniels, A. Cupo, V. Meunier, X. Feng, A. Narita *et al.*, Engineering of robust topological quantum phases in graphene nanoribbons, Nature (London) **560**, 209 (2018).

[3] D. J. Rizzo, J. Jiang, D. Joshi, G. Veber, C. Bronner, R. A. Durr, P. H. Jacobse, T. Cao, A. Kalayjian, H. Rodriguez *et al.*, Rationally designed topological quantum dots in bottom-up graphene nanoribbons, ACS Nano **15**, 20633 (2021).

[4] K. Wakabayashi, K. ichi Sasaki, T. Nakanishi, and T. Enoki, Electronic states of graphene nanoribbons and analytical solutions, Sci. Technol. Adv. Mater. **11**, 054504 (2010).

[5] M. Ezawa, Exact solutions for two-dimensional topological superconductors: Hubbard interaction induced spontaneous symmetry breaking, Phys. Rev. B **97**, 241113(R) (2018).

[6] S. R. Eric Yang, M.-C. Cha, H. J. Lee, and Y. H. Kim, Topologically ordered zigzag nanoribbon: $e/2$ fractional edge charge, spin-charge separation, and ground state degeneracy, Phys. Rev. Res. **2**, 033109 (2020).

[7] I. H. Lee, H. A. Le, and S. R. E. Yang, Mutual information and correlations across topological phase transitions in topologically ordered graphene zigzag nanoribbons, Entropy **25**, 1449 (2023).

[8] T. Cao, F. Zhao, and S. G. Louie, Topological phases in graphene nanoribbons: Junction states, spin centers, and quantum spin chains, Phys. Rev. Lett. **119**, 076401 (2017).

[9] T. Luu, U.-G. Meißner, and L. Razmadze, Localization of electronic states in hybrid nanoribbons in the nonperturbative regime, Phys. Rev. B **106**, 195422 (2022).

[10] A. Honet, L. Henrard, and V. Meunier, Robust correlated magnetic moments in end-modified graphene nanoribbons, arXiv:2310.09057.

[11] H. C. Lee and S. R. Eric Yang, Chiral symmetry breaking and topological charge of zigzag graphene nanoribbons, New J. Phys. **26**, 033039 (2024).

[12] P. R. Wallace, The band theory of graphite, Phys. Rev. **71**, 622 (1947).

[13] R. Kundu, Tight-binding parameters for graphene, Mod. Phys. Lett. B **25**, 163 (2011).

[14] J.-W. Rhim, J. Behrends, and J. H. Bardarson, Bulk-boundary correspondence from the intercellular Zak phase, Phys. Rev. B **95**, 035421 (2017).

[15] Exactly how long each segment needs to be to exhibit such a simple decay is not clear *a priori*. While we only intend to describe asymptotic behavior, in practice $m \gtrsim 3$ appears to suffice.

[16] Mount Kilimanjaro in Tanzania has an extended high plateau, while the Japanese mount Fuji features a sharp peak. The resemblances to the respective localizations inspired the naming scheme.

[17] With open boundary conditions we always find two degenerate zero-energy states that correspond to perfect localizations on the extreme ends of the system. These states play no role in the limit of semi-infinite ends, as their localizations are pushed to infinity. The relevant states are the lowest nonzero energy states, which we show in Fig. 6.

[18] N. N. Bogoljubov, On a new method in the theory of superconductivity, Il Nuovo Cimento **7**, 794 (1958).

[19] Crommie Research Group, Topological Engineering of GNRs (2019), https://physics.berkeley.edu/research-faculty/crommie-group/research/topology-and-bottom-synthesis-graphene-nanoribbons-gnrs-1 accessed 2023-12-31.